CeO₂/Pt/Al₂O₃ catalysts for the WGS reaction: Improving understanding of the Pt-O-Ce-Ox interface as an active site

Laís Reis Borges [a,b], Adriano H. Braga [a,b], Daniela Zanchet [a,b], Jean Marcel R. Gallo [a,b], José Maria C. Bueno [a,b,*]

[a] Department of Chemical Engineering, Federal University of São Carlos, P.O. Box 676, 13565-905 São Carlos, SP, Brazil
[b] Institute of Chemistry, University of Campinas – UNICAMP, P.O. Box 6154, 13083-970 Campinas, SP, Brazil

ABSTRACT

In this work, we demonstrate that knowledge of the structural parameters of Pt nanoparticles (PtNp) supported on ceria/alumina is essential for understanding the surface structure, the electronic properties of PtNp, and the effect of ceria on the catalytic activity in the water-gas shift reaction. The similar Pt-Pt and Pt-O bond distances for different PtNp sizes suggested similar electronic density of the Pt sites, indicating that changes of the electronic properties of the Pt sites, due to the size effect, were compensated by the presence of Pt-O species. The turnover frequency based on Pt⁰ sites varied between 2 and 10 times higher, compared to unpromoted catalysts, and was dependent on the PtNp size and morphology, which determined the density of oxygen on the surface and the density of Pt-O-Ce sites. The effect of ceria in increasing the activity could be explained by the creation of active Pt-O-Ce sites at the surface.

1. Introduction

Metal nanoparticles with sizes usually in the range 1–100 nm, dispersed on oxides, are used in several industrial processes [1–4]. The size of the metal nanoparticles and the nature of the support are factors that influence the catalytic activity. In the last decade, solid theoretical and experimental studies have unveiled the fundamental aspects of metal particle size and metal-support interaction. In previous work by our group, we demonstrated that for oxophilic metals such as Co, [1] Cu, [2] and Pt [3], the presence of oxygen at the metal surface, besides participating in metal-support interaction (M-O-Sup), modifies the electronic properties of the accessible metal sites and significantly affects the catalytic properties. The changes in activity may be dependent on the metal nanoparticle size and the nature of the metal: i) in the case of cobalt-based catalysts for steam reforming of ethanol, the thickness of the Co−O shell formed on a reduced core controlled the reactivity of the metal-metal oxide surface and decreased the rate of carbon accumulation; [1] ii) the oxidation of CO by H₂O over Cu/Al₂O₃ catalysts was size-dependent, with the Cu-O interface having direct participation in the turnover frequency (TOF). The presence of Cu₂-O species on the Cu surface decreased for larger particles and modified the electronic properties of the Cu active sites, which was reflected in higher activity;

[2] iii) for Pt/Al₂O₃ catalysts, on the other hand, the oxygen coverage of the Pt nanoparticles did not affect the surface electronic properties, due to a compensation effect between the size of the Pt⁰ core and oxygen coordinated on the shell [3]. However, it is known that in some reactions, high activity can be obtained by associating a specific support [5]. An example is the water-gas shift reaction (WGSR) catalyzed by a metal such as Pt [4] or Cu, [2] in the form of metal/Al₂O₃, where the presence of cerium significantly increases the reaction rates.

The WGSR is an important step in hydrogen production and is widely used in processes such as ammonia synthesis and the hydrotreatment of fuels, so it is essential to understand and improve the catalysts employed in this reaction [6]. Catalysts based on platinum supported on a reducible metal oxides, such as TiO₂ or CeO₂, have received much attention, due to their potential applications in fuel cells. Consequently, various experimental and theoretical studies have investigated ways to maximize the activity of the Pt sites [7–11]. The effect of ceria has been extensively discussed, with wide acceptance of the importance of oxygen vacancies in ceria-based catalysts [12–14]. The metal-ceria interaction can change the Pt phase, affecting the stability of the metal particle, which can be reflected in a smaller metal particle size, depending on the atmosphere and temperature [9,10,14–16]. Structural changes of the Pt particles, together with modifications of the electronic

properties of both ceria and Pt, were observed after Pt deposition and after heating [17]. Nevertheless, there is still much debate concerning the identification of highly active sites on Pt/ceria catalysts used for the WGS reaction and low-temperature CO oxidation [18]. Experimental studies of Pt/CeO$_2$ catalysts suggest a redox mechanism, with the presence of inactive formate and carbonate surface species [18,19]. A redox mechanism involving formate and $-$OH group regeneration has also been proposed for the Pt/CeO$_2$ catalyst [19,20]. Overall, the studies suggest that the WGSR mechanism and activity depend on the presence of the CeO$_2$ and the size of the Pt particles. A detailed investigation of the structural and electronic properties of Pt/CeO$_2$-Al$_2$O$_3$ catalysts, based on the results of both *ex situ* and *in situ* experiments and using pre-made Pt nanoparticles with average particle size of 2.8 nm, did not find a direct correlation between catalytic activity and the ceria properties. The main parameter affecting the activity seemed to be the ceria loading [21]. Computational studies of the WGSR on Pt clusters supported on CeO$_2$ have tried to solve issues concerning the activity and the mechanism, using a molecular level understanding of each component at the metal/oxide interface sites [11]. Activation of H$_2$O is an important step in both the redox and associative pathways, and various studies based on different metals and metal/oxide interfaces have indicated the H$_2$O dissociation as a rate-controlling step [20,22–24].

Considering that Pt is an expensive noble metal, there is great interest in obtaining Pt-based catalysts that maximize the Pt dispersion, approaching single atoms [25,26]. In our previous studies, we demonstrated that for Pt/Al$_2$O$_3$ catalysts, the coverage of Pt by oxygen increased with decreasing metal particle size, with Pt^{2+} stabilized on the Pt nanoparticle surface [3]. It is worth noting that most experimental studies have utilized Pt nanoparticles larger than 2 nm, which is expected to lead to lower interaction with oxygen [27–30]. The structure of the oxygen-containing surface has not been considered in the characterization of Pt nanoparticles, although it could not only promote interactions with the support, but also provide the possibility of anchoring CeO$_x$ species, creating a unique Pt-CeO$_x$ interface.

In this work, as a strategy to understand the effect of the surface structure of Pt nanoparticles on the interaction with ceria and its activity in the WGSR, Pt nanoparticles < 1.5 nm were synthesized on alumina and modified with ceria. The Pt nanoparticles were sufficiently small to allow a high concentration of Pt-O species on the Pt surface. Determination of the structural parameters of Pt by X-ray absorption fine structure spectroscopy (XAFS) enabled modeling of the surface structure of the Pt nanoparticles. The results provided insightful information about the role of the surface structure of the Pt particles forming an interface with ceria, which is crucial for obtaining catalysts with high activity in the WGSR.

2. Material and methods

2.1. Catalyst preparation

The γ-Al$_2$O$_3$ support, synthesized by the sol-gel method, [31] was crushed, sieved (<100 mesh), and calcined for 4 h at 500 °C (4 °C min^{-1}), under a flow of synthetic air. The PtAl and PtAl_Cl catalysts [3] were modified by the addition of ceria, with impregnation using an aqueous solution of Ce(NO$_3$)$_3$0.6 H$_2$O precursor, followed by drying (100 °C, 10 h) and calcination under a flow of synthetic air (500 °C, 4 h). The catalysts were denoted *y*Ce*x*PtAl and *y*Ce*x*PtAl_Cl, for the materials produced using the precursors Pt(NH$_3$)$_4$(NO$_3$)$_2$ and H$_2$PtCl$_6$, respectively, where *x* and *y* are the nominal platinum and ceria mass percentages, respectively (*x* = 0.3, 0.5, 1, and 2 wt %; *y* = 0, 3, 6, and 10 wt %).

2.2. Catalyst characterization

The metal loadings of the calcined catalysts, before and after a reducing treatment (at 500 °C for 1 h, under a flow of H$_2$), were determined by energy dispersive X-ray fluorescence (XRF) analyses, using a Shimadzu EDX700 spectrometer.

Powder X-ray diffraction (XRD) analyses employed a Rigaku Multiflex diffractometer with Ni filter and Cu Kα radiation (λ = 1.5442 Å), operated at 40 kV and 30 mA. The data were acquired from 10° to 90°, with a scan rate of 2° min^{-1}. The crystallite sizes were determined by the Scherrer equation.

Temperature-programmed reduction with H$_2$ (H$_2$-TPR) analyses were performed using a Micromeritics AutoChem 2920 instrument. The catalyst (60 mg) was dried for 30 min at 150 °C, under a flow of N$_2$. After cooling to room temperature, the sample was heated to 900 °C, at 10 °C. min^{-1}, under a 30 mL min^{-1} flow of 10 % H$_2$/N$_2$. The H$_2$ uptake was monitored using a thermal conductivity detector (TCD).

Fourier transform infrared spectroscopy with CO adsorption (FTIR-CO) analyses employed a Thermo Nicolet iS50FTIR spectrometer equipped with an MCT detector and a transmission cell (Harrick) with CaF$_2$ windows. Disks of the samples (~10 mg) were pre-reduced for 1 h at 500 °C, with heating at 10 °C.min^{-1}, under a 35 mL.min^{-1} flow of 30 % H$_2$/He. After cooling to room temperature under a flow of He, the sample was exposed to a 2 mL.min^{-1} flow of CO, at 20 Torr, for 10 min. The FTIR spectra (average of 64 scans with resolution of 4 cm^{-1}) were collected until complete saturation of the catalyst surface, followed by purging with a 20 mL.min^{-1} flow of He. The mols of Pt at the surface were estimated by deconvolution of the CO adsorption peak area, using a Gaussian curve and a conversion factor obtained by calibration with a known dispersion of catalyst standard (Pt/Al$_2$O$_3$).

In situ diffuse reflectance infrared Fourier transform spectroscopy (*in situ* DRIFTS) measurements were performed under WGSR conditions, using a Thermo Nicolet iS50FTIR spectrometer equipped with an MCT detector and a Harrick DRIFTS cell with CaF$_2$ windows. The samples were pre-reduced for 1 h at 500 °C, with heating at 10 °C.min^{-1}, under a 35 mL.min^{-1} flow of 30 % H$_2$/He, followed by cooling to 250 °C under a flow of He. At 250 °C, the samples were submitted to WGSR conditions (CO:H$_2$O = 1:3) and the temperature was increased to 350 °C, in steps of 50 °C. The *in situ* DRIFTS spectra (average of 64 scans with resolution of 4 cm^{-1}) were collected every 5 min, during 30 min at each temperature.

XAFS analyses at the Pt L$_3$-edge (11,564 eV) were carried out at the D08B-XAFS2 beamline of the Brazilian Synchrotron Light Laboratory (LNLS, Campinas, Brazil), using an Si(111) double crystal monochromator. The sample data were collected in fluorescence mode, using a Kapton window and 8-element Ge detector. XANES spectra were collected during *in situ* reduction at 500 °C for 1 h, under a 100 mL. min^{-1} flow of 5 % H$_2$/He. Subsequently, the sample was cooled to room temperature, under H$_2$, and the EXAFS data were acquired (k$_{max}$ = 14 Å^{-1}). The IFEFFIT software package [32] was used to analyze the XANES and EXAFS data. A window of k = 3–12 Å^{-1} was used for the Fourier transformation. The passive electron amplitude reduction factor (S$_0^2$) and the photoelectron energy origin correction (E$_0$) were determined for the standards (Pt^0 and PtO$_2$) and were used in the sample fittings. Linear combination analysis (LCA) of the XANES spectra was used to estimate the percentages of the Pt^0 and Pt-O species in the catalyst after the reduction.

XAFS analyses at the Ce L$_3$-edge (5723 eV) were carried out at the same beamline in transmission mode. The XANES measurements was performed during the same *in situ* reduction described above. Metallic chromium was used as a reference for energy calibration. The fractions of Ce^{3+} and Ce^{4+} species were estimated by the peak fitting method, [2] where the electronic transitions were represented by five Gaussian functions and an arctangent function. These analyses were performed with WinXAS 3.1 software.

Scanning transmission electron microscopy with high-angle angular dark-field scanning detection (HAADF-STEM) employed a TECNAI G2F20 instrument equipped with a field emission gun, operated at 200 kV. The diameters of the nanoparticles were determined using ImageJ software, with calculation of the average Pt particle size.

2.3. Catalytic tests

Measurements of catalytic activity were carried out using a continuous-flow tubular fixed-bed quartz reactor, at atmospheric pressure. The samples were reduced for 1 h at 500 °C, with heating at 10 °C. min^{-1}, under a 35 mL min^{-1} flow of H$_2$. The catalytic tests were performed from 200° to 400°C, with steps of 50 °C, using a space velocity of 0.036 g.s.mL, with a feed consisting of 5 % CO, 15 % H$_2$O, and He balance. Water steam was introduced into the reactor by bubbling He through a water saturator at 65 °C. The reaction products were analyzed by online gas chromatography, using a Bruker 450 instrument equipped with two TCDs and Porapak Q and molecular sieve 13X columns. The forward rate (R$_f$) was determined from the observed rate (R$_{obs}$), using the following equation:

$$R_f = \frac{R_{obs}.(P_{CO}P_{H_2O})_{feed}}{\left[(P_{CO}P_{H_2O})_{out} - \left(\frac{P_{CO_2}P_{H_2)out}}{K_{eq}}\right)_{out}\right]} \tag{1}$$

For higher activity samples, the R$_f$ values were estimated using CO conversion of X$_{CO}$ = 15 %, as shown in Table S6. The forward turnover frequency (TOF$_f$) at 300 °C was based on the forward rate per surface Pt^0 atom on the particles. The estimation of the amount of surface platinum sites corresponded to the number of CO molecules covering the metal at saturation, obtained from the FTIR-CO analysis (considering the CO/Pt adsorption stoichiometry to be equal to 1) [33].

3. Results and discussion

3.1. Catalyst characterization

The XRF elemental analyses of the *yCexPtAl* and *yCexPtAl_Cl* catalysts are reported in Table S1, including the Cl/Pt ratios for the calcined and reduced *yCexPtAl_Cl* catalysts. The Pt and Ce loadings were comparable to the nominal values, with the Pt loading slightly decreasing with increase of the ceria content in both series. As observed for the *xPtAl_Cl* catalysts, the chlorine was retained in the yCexPtAl_Cl catalysts and increased with Pt loading.

The physicochemical properties of the *yCexPtAl_Cl* and *yCexPtAl* catalysts are shown in Table S2. The specific surface area (S$_{BET}$) varied between 208 and 314 m^2.g^{-1}, while the pore volume (V$_p$) ranged between 0.23 and 0.35 cm^3 g^{-1}. For the *yCexPtAl* samples, the S$_{BET}$ and V$_p$ indicated that the porous structure of the Al$_2$O$_3$ support was maintained after impregnation with Pt and ceria. For the *xPtAl_Cl* catalyst series, the S$_{BET}$ and V$_p$ values were dependent on the Pt loading, which could indicate hydrolysis of the alumina by the H$_2$PtCl$_6$.

The X-ray diffraction patterns are shown in Fig. S1. All the samples presented broad peaks attributed to the γ-Al$_2$O$_3$ support, while the Pt species Pt^0, PtO, and PtO$_2$ were not detected, indicating that the Pt was well dispersed. The CeO$_2$ fluorite phase (JCPDS 00–004–0593; 2θ = 28.5; 33.3; 47.5; 56.4°) was detected in all the catalysts (*yCexPtAl* and *yCexPtAl_Cl*), except for the 3Ce*x*PtAl samples, where the lack of long-range order suggested that the ceria crystallites were better dispersed. For the samples in which the CeO$_2$ fluorite phase was detected, the average crystallite size was calculated using the Scherrer equation (Table S3). The CeO$_2$ crystallite sizes (D$_{CeO2}$) detectable by XRD were
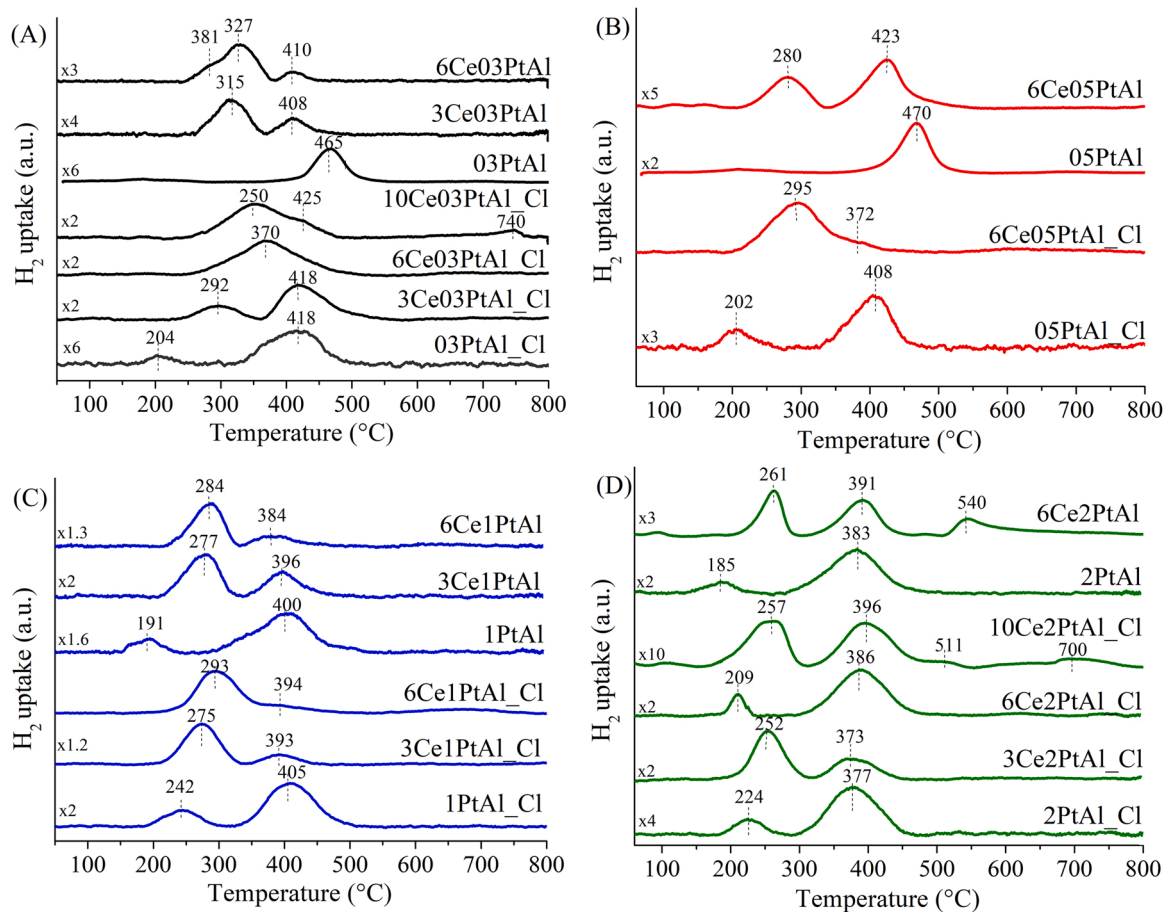

Fig. 1. H$_2$ uptakes of the catalysts (A) *y*Ce03PtAl_Cl and *y*Ce03PtAl, (B) *y*Ce05PtAl_Cl and *y*Ce05PtAl, (C) *y*Ce1PtAl_Cl and *y*Ce1PtAl, and (D) *y*Ce2PtAl_Cl and *y*Ce2PtAl, during temperature-programmed reduction.

larger than the alumina pore size (t_p) (Table S2), suggesting that the larger fluorite crystallites grew externally, outside the support pores. For the chlorinated samples, the ceria fluorite crystallite sizes detectable by XRD were slightly smaller than for the non-chlorinated samples (for example, around 6 and 7 nm for the 6CexPtAl_Cl and 6CexPtAl samples, respectively).

The H_2 uptake profiles (Fig. 1) showed two main features, corresponding to a low temperature reduction (LTR), at around 200 °C, and a high temperature reduction (HTR), at around 400 °C. The peaks at 200 and 400 °C could be ascribed to different species of platinum oxide and were affected by the Pt loading, in agreement with previous results [3]. For the xPtAl samples, the reduction peaks were expected to occur, due to the reduction of PtO$_x$ associated with the phenomenon of H-spillover from Pt to Al$_2$O$_3$, resulting in a slightly higher H_2 absorption value, compared to the corresponding PtO$_x$ species [34,35].

For Ce-containing catalysts, with reduction of PtO$_x$ species, the Pt^0 acts as H_2 activation sites (Pt-H) and modifies the oxide structures by hydrogen spillover. The reduction of bulk ceria, which has been reported to occur at 750 °C, was only detected for the 10CexPtAl_Cl, while surface ceria reduction occurred between 400 and 500 °C, [36] facilitated by interaction with noble metals [37]. Previous work observed the improvement of ceria reducibility due to metal-CeO$_2$ interaction, [38] so the HTR could be explained by the contact between surface ceria and the metal [39]. Therefore, the features observed below 500 °C could correspond to the reduction of platinum oxides, as well as surface ceria by means of the H-spillover effect. The quantification of hydrogen uptake (μmol.g$_{cat}^{-1}$) based on the peaks below 500 °C is shown in Table S3. The H_2 uptake increased with the ceria loading, with values of 76, 163, 186, and 199 μmol.g$_{cat}^{-1}$ for the 0.3PtAl_Cl, 3Ce03PtAl_Cl, 6Ce03PtAl_Cl, and 10Ce03PtAl_Cl catalysts, respectively, suggesting that the ceria was also reduced at temperature lower than 500 °C. For the xPtAl sample series, the addition of ceria generally facilitated the reduction of species that reduce at high temperature, as shown in Fig. 1A–D.

The reduction temperature was also modified by increase of the Pt loading, for the same ceria content. For the 6CexPtAl samples, increase of the Pt loading led to a tendency of the LTR to shift to lower temperatures (327, 280, 284, and 260 °C for 6Ce03PtAl, 6Ce05PtAl, 6Ce1PtAl, and 6Ce2PtAl, respectively). It is reasonable to suppose that the increase of the PtO$_x$ nanoparticle size with Pt loading would imply, due to the effect of increase of the PtO size, a smaller fraction of the Pt particles with lower interaction with the support, which would favor the reduction. As mentioned above, while ceria could promote Pt dispersion and increase the oxygen vacancies, [40] facilitating reduction of the oxides, similar to the behavior described for NiO, [40] it could also affect the strength of the metal-support interactions, [41] hindering PtO$_x$ reduction, with the effect varying according to the Pt and ceria loading. Hence, it was not possible to determine the parameter responsible for H_2 activation.

The samples with high Pt and Ce loadings, such as the 6Ce2PtAl and 10Ce2PtAl_Cl catalysts, also presented H_2 uptake at around 500–550 °C (Fig. 1D). This could be assigned to a nonstoichiometric cerium oxide, [42] indicating low Pt-O-Ce interaction, due to difficulty in transferring oxygen from the oxide to reduce the surface Pt-CeO$_x$ [43]. For the 10Ce03PtAl_Cl and 10Ce2PtAl_Cl catalysts, H_2 uptake at around 700 °C could be assigned to reduction of the bulk ceria, [36] or to the formation of CeAlO$_3$ from ceria dispersed on the alumina [42].

For the chlorinated samples (yCexPtAl_Cl), a single broad reduction peak at low Pt loading suggested a uniform reduction of CeO$_x$ and PtO$_x$ species, as indicated by peaks at 370, 250, and 295 °C for the 6Ce03PtAl_Cl, 10Ce03PtAl_Cl, and 6Ce05PtAl_Cl catalysts, respectively (Fig. 1A and B). Increase of the Pt and Ce loadings in the yCexPtAl_Cl samples could lead to the formation of CeOCl [44] or Ce(OH)$_2$Cl species [45] by substitution of oxygen ions of the ceria lattice by Cl during the reduction treatments; this would also decrease hydrogen chemisorption on the ceria, [43,46] hindering the spillover process. For the chlorinated samples with high Pt contents, the LTR shifted to lower temperature

with increase of the ceria loading, as indicated by peaks at 252 and 209 °C for the 3Ce2PtAl_Cl and 6Ce2PtAl_Cl catalysts, respectively. This could indicate the influence of a high content of residual chlorine on PtO$_x$ particle size and/or metal-support interaction.

The effect of the ceria on the surface structure of the platinum particles was investigated by FTIR-CO (Fig. 2A–D), with the deconvoluted spectra shown in Figs. S2-S4. The spectra indicated the presence of different Pt species, according to the Pt and Ce loadings. A band at 1807 cm^{-1} in the low frequency (LF) region was characteristic of Pt-CO in bridge mode, while a band at 2084–2025 cm^{-1} in the high frequency (HF) region was characteristic of on-top CO adsorption at Pt^0 sites, as reported previously for PtAl and PtAl_Cl catalysts [3].

The addition of ceria to the Cl-free samples with low Pt loading (xCe03PtAl and xCe05PtAl) resulted in a main band at around 2068 cm^{-1}, with a tail at around 2025 cm^{-1}, (Fig. 2A and B), suggesting that the Pt^0 sites had similar electronic properties for these catalysts with different ceria loadings. For the samples with high Pt loading (xCe1PtAl and xCe2PtAl), the HF region showed signals corresponding to CO species at 2025, 2051, and 2068 cm^{-1} (Fig. 2C and D), which depended on the ceria loading. Increase of the ceria loading led to a blue-shift of on-top Pt^0-CO species, [47] as shown by signals at 2051 cm^{-1} for 1PtAl and 2068 cm^{-1} for 6Ce1PtAl, with clear decrease of the tail at around 2025 cm^{-1}, as well as by signals at 2025 cm^{-1} for 2PtAl and 2051 cm^{-1} for 6Ce2PtAl. The shift to higher frequency could indicate a major contribution of high coordination Pt [48] and the presence of low defect terrace sites [49]. In addition to the shift of the main band to higher frequency, there was increased intensity of the band at 2084 cm^{-1}, corresponding to CO bonded linearly to electron-deficient platinum, such as Pt$^{\delta+}$ ($1 > \delta$) [3,50]. For high Pt loading samples (xCe1PtAl and xCe2PtAl) (Fig. 2C and 2D), the band in the LF region at 1807 cm^{-1}, attributed to bridge Pt(CO)$_2$ species, was suppressed with increase of the ceria loading. These results suggested significant changes of the surface structure due to the presence of ceria in the samples with > 1 wt % Pt loading.

The trend of CO adsorption on the Pt surfaces induced by ceria was similar for the yCexPtAl and yCexPtAl_Cl catalyst series. However, at higher Pt loading, there was a pronounced difference in the main frequency between the Cl-containing samples and the Cl-free samples, as shown for 6Ce2PtAl (2051 cm^{-1}) and 6Ce2PtAl_Cl (2068 cm^{-1}) (Fig. 2D). This shift to higher frequency suggested significant differences in morphology due to the presence of chlorine.

No bands were detected corresponding to CO adsorption at the metal-support interface (C bonded to the metal and O bonded to the oxide, at 1740 cm^{-1} [51]) or for CO adsorbed on Ce(IV) and Ce(III) sites, [49,51] since the CO was preferentially adsorbed on Pt sites [52]. Interestingly, the suppression of bands for highly coordinated Pt(CO) [2,3] species suggested the presence of defects on the surfaces of the smaller Pt particles stabilized by the presence of ceria by means of the Pt-O-Ce interaction [53–55]. The large difference of the extinction co-efficient between the linear Pt-CO and high coordination species [2,3] together with suppression of the high-coordination species by the presence of ceria, enabled accurate determination of the fraction of Pt^0 on the surfaces of the Ce-containing catalysts, based on the band for linearly adsorbed CO. The fractions of Pt^0 sites at the surface (θ_{Pt}^0) are shown in Table S4. Interestingly, for the Cl-containing samples, the θ_{Pt}^0 value increased with increase of the ceria loading, while the opposite behavior was observed for the Cl-free samples.

For better understanding of the effect of ceria on the Pt surface structure, XAFS was used to investigate the structural changes caused by CeO$_2$ addition to the catalysts. The EXAFS results collected at room temperature for the reduced catalysts are shown in Table 1 and Table 2. The corresponding spectra in k and R space, together with the best fits, are displayed in Figs. S5-S7. The Pt-Pt and Pt-O scattering paths of the first shell, referenced to Pt foil [56] and PtO$_2$, [57] were considered in the analysis. The parameters determined were the coordination numbers (N_{Pt-Pt} and N_{Pt-O}), the bond lengths (R_{Pt-Pt} and R_{Pt-O}), the Debye-Waller

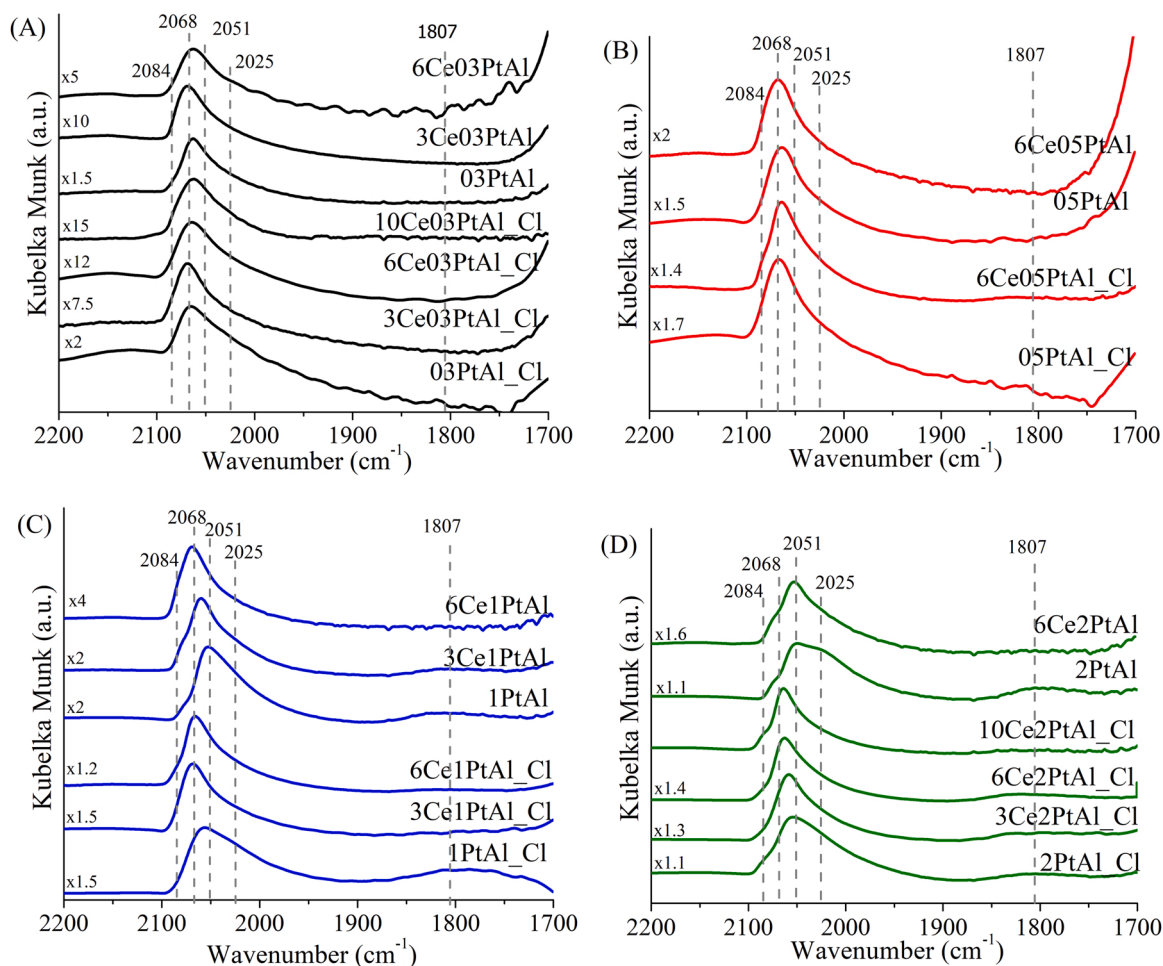**Fig. 2.** Normalized FTIR-CO adsorption spectra for the reduced samples: (A) *y*Ce03PtAl_Cl and *y*Ce03PtAl; (B) *y*Ce05PtAl_Cl and *y*Ce05PtAl; (C) *y*Ce1PtAl_Cl and *y*Ce1PtAl; (D) *y*Ce2PtAl_Cl and *y*Ce2PtAl.

Table 1
Structural parameters obtained from EXAFS data acquired at room temperature for the *y*Ce*x*PtAl_Cl catalysts after reduction in H_2 at 500 °C.

Sample	N_{Pt-Pt}	R_{Pt-Pt} (Å)	N_{Pt-O}	R_{Pt-O} (Å)	σ^2_{Pt-Pt} (x10^{-3}) (Å^2)	σ^2_{Pt-O} (x10^{-3}) (Å^2)	D_{Pt} (nm)
03PtAl_Cl[a]	8.10 ± 0.01	2.75 ± 0.001	0.73 ± 0.07	1.99 ± 0.01	5.51 ± 0.12	8.23 ± 1.57	1.3[b]
3Ce03PtAl_Cl	7.99 ± 0.35	2.74 ± 0.003	1.04 ± 0.12	2.01 ± 0.01	7.95 ± 0.35	8.23 ± 1.57	1.2[b]
6Ce03PtAl_Cl	6.21 ± 0.42	2.74 ± 0.004	1.26 ± 0.16	2.01 ± 0.01	7.64 ± 0.50	8.23 ± 1.57	0.9[b] 1.0 ± 0.2[c]
05PtAl_Cl[a]	8.23 ± 0.01	2.75 ± 0.002	0.56 ± 0.07	2.02 ± 0.02	5.89 ± 0.32	8.23 ± 1.57	1.4[b]
6Ce05PtAl_Cl	7.28 ± 0.53	2.75 ± 0.004	1.19 ± 0.18	2.01 ± 0.01	8.14 ± 0.56	8.23 ± 1.57	1.1[b]
1PtAl_Cl[a]	8.35 ± 0.04	2.75 ± 0.002	0.45 ± 0.09	2.02 ± 0.02	6.56 ± 0.20	8.23 ± 1.57	1.4[b] 1.3 ± 0.4[c]
3Ce1PtAl_Cl	7.08 ± 0.36	2.74 ± 0.003	1.20 ± 0.16	2.00 ± 0.01	5.71 ± 0.35	8.23 ± 1.57	1.1[b]
6Ce1PAl_Cl	5.56 ± 0.32	2.74 ± 0.004	1.16 ± 0.11	2.01 ± 0.01	5.71 ± 0.40	8.23 ± 1.57	0.9[b] 1.0 ± 0.2[c]
2PtAl_Cl[a]	8.40 ± 0.09	2.75 ± 0.001	0.18 ± 0.04	2.04 ± 0.02	5.08 ± 0.15	8.23 ± 1.57	1.4[b] 1.4 ± 0.6[c]
3Ce2PtAl_Cl	7.38 ± 0.22	2.74 ± 0.001	0.55 ± 0.09	2.02 ± 0.02	6.09 ± 0.21	8.23 ± 1.57	1.1[b] 1.0 ± 0.2[c]
6Ce2PtAl_Cl	7.04 ± 0.22	2.74 ± 0.002	0.48 ± 0.07	2.00 ± 0.02	7.93 ± 0.25	8.23 ± 1.57	1.1[b] 1.1 ± 0.1[c]
10Ce2PtAl_Cl	5.54 ± 0.43	2.73 ± 0.006	1.04 ± 0.13	2.01 ± 0.01	9.72 ± 0.68	8.23 ± 1.57	0.8[b]

[a] Reported in Ref. [3].
[b] Average Pt particle diameter obtained by EXAFS correlation [58].
[c] Average Pt particle diameter obtained by HAADF-STEM. Standards data: Pt^0: $E_{0\ (Pt-Pt)}$ = 8 eV; $S^2_{0\ (Pt-Pt)}$ = 0.8; R_{Pt-Pt} = 2.77 ± 0.004 Å. PtO$_2$: $E_{0\ (Pt-O)}$ = 11.5 eV; $S^2_{0\ (Pt-O)}$ = 0.9; R_{Pt-O} = 2.01 ± 0.03 Å.

scattering coefficients (σ^2_{Pt-Pt} and σ^2_{Pt-O}), and the particle sizes provided from the cuboctahedral model by N_{Pt-Pt} [58].

Interestingly, the Cl-containing catalysts (*x*PtAl_Cl) showed higher N_{Pt-Pt} of around 8, compared to the Cl-free samples (*x*PtAl) with very low N_{Pt-Pt} of around 4. The *x*PtAl_Cl catalyst series showed a slight increase of N_{Pt-Pt} with Pt loading (for 03PtAl_Cl, N_{Pt-Pt} = 8.10 ± 0.01; for 2PtAl_Cl, N_{Pt-Pt} = 8.40 ± 0.09). Similar behavior was observed for the Cl-free catalysts (for 03PtAl, N_{Pt-Pt} = 4.40 ± 0.03; for 2PtAl, N_{Pt-Pt} =

4.62 ± 0.39).

For both the Cl-containing and Cl-free samples, the addition of Ce and increase of the Ce loading led to a monotonic decrease of the Pt-Pt coordination number (N_{Pt-Pt}) and an increase of the Pt-O coordination number (N_{Pt-O}). The N_{Pt-Pt} values were 4.5, 3.7, and 3.6, while the N_{Pt-O} values were 1.67 ± 0.12, 2.13 ± 0.14, and 2.17 ± 0.42, for the 1PtAl, 3Ce1PtAl, and 6Ce1PtAl catalysts, respectively. The differences were more pronounced for the Cl-containing samples, with N_{Pt-Pt} values of

Table 2

Structural parameters obtained from EXAFS data acquired at room temperature for the $yCexPtAl$ catalysts after reduction in H_2 at 500 °C.

Sample	N_{Pt-Pt}	R_{Pt-Pt} (Å)	N_{Pt-O}	R_{Pt-O} (Å)	σ^2_{Pt-Pt} (x10^{-3}) (Å^2)	σ^2_{Pt-O} (x10^{-3}) (Å^2)	D_{Pt} (nm)
03PtAl[a]	4.40 ± 0.03	2.75 ± 0.004	1.78 ± 0.13	1.99 ± 0.01	4.65 ± 0.45	3.72 ± 0.92	0.7[b]
3Ce03PtAl	4.15 ± 0.48	2.75 ± 0.001	2.06 ± 0.14	2.00 ± 0.01	6.55 ± 0.83	3.72 ± 0.92	0.7[b]
1PtAl[a]	4.51 ± 0.31	2.75 ± 0.004	1.67 ± 0.12	2.01 ± 0.01	5.50 ± 0.46	3.72 ± 0.92	0.7[b] 1.1 ± 0.2[c]
3Ce1PtAl	3.65 ± 0.44	2.75 ± 0.001	2.13 ± 0.14	2.01 ± 0.01	6.33 ± 0.87	3.72 ± 0.92	0.7[b]
6Ce1PtAl	3.60 ± 0.07	2.75 ± 0.001	2.17 ± 0.42	2.00 ± 0.02	7.24 ± 2.37	3.72 ± 0.92	0.7[b]
2PtAl[a]	4.62 ± 0.39	2.75 ± 0.001	1.24 ± 0.13	1.99 ± 0.01	6.29 ± 0.61	3.72 ± 0.92	0.8[b] 1.2 ± 0.2[c]
6Ce2PtAl	4.60 ± 0.04	2.74 ± 0.004	1.41 ± 0.12	2.00 ± 0.01	7.48 ± 0.72	3.72 ± 0.92	0.7[b] 1.0 ± 0.2[c]

[a] Reported in Ref. [3].

[b] Average Pt particle diameter obtained by EXAFS correlation [58].

[c] Average Pt particle diameter obtained by HAADF-STEM. Standards data: Pt^0: $E_{0 (Pt-Pt)}$ = 8 eV; S_0^2 $_{(Pt-Pt)}$ = 0.8; R_{Pt-Pt} = 2.77 ± 0.004 Å. PtO$_2$: $E_{0 (Pt-O)}$ = 11.5 eV; S_0^2 $_{(Pt-O)}$ = 0.9; R_{Pt-O} = 2.01 ± 0.03 Å.

8.35 ± 0.04, 7.08 ± 0.36, and 5.56 ± 0.32, and N_{Pt-O} values of 0.45 ± 0.09, 1.20 ± 0.16, and 1.16 ± 0.11, for the 1PtAl_Cl, 3Ce1PtAl_Cl, and 6Ce1PtAl_Cl catalysts, respectively. As reported elsewhere, [15] decrease of the Pt-Pt coordination number with ceria loading indicates the stabilization of small Pt clusters when the Al_2O_3 surface is modified by CeO_x. This suggests that growth of Pt is suppressed due to alteration of Pt diffusion in the presence of ceria, resulting in a smaller Pt particle size (D_{Pt}), [15,58] as supported by the results shown in Table 3. Furthermore, the reduction degree is directly correlated with the Pt particle size, decreasing with lower D_{Pt}, meaning that the free energy of the $Pt_n + O_x \leftrightarrow Pt_{(n-x)}PtO_{x/2}$ reaction increases with increase of the surface curvature, [29] resulting in substantially higher surface reactivity of small particles towards oxygen (Pt-O-Pt interaction). The increase of Pt-O coordination with addition of ceria could also lead to interaction with ceria by Pt-O-Ce bonding, [15] with the platinum interacting with ceria through the lattice oxygen on the surface. It is important to note that the presence of ceria could enhance the oxygen density for each platinum atom, since the Pt-O-Ce interaction involves one oxygen atom bonded to one platinum atom, whereas the Pt-O-Pt interaction consists of one oxygen atom bonded to two platinum atoms. Therefore, the presence of ceria leads to higher sensitivity of the platinum atom charge to the oxygen at the metal-support interface.

The Cl-containing samples promoted with Ce ($yCexPtAl\_Cl$) showed higher N_{Pt-Pt} and lower N_{Pt-O}, compared to the Cl-free samples ($yCexPtAl$), as observed for the $xPtAl$ and $xPtAl\_Cl$ samples [3]. For the $yCexPtAl$ samples, the decrease of N_{Pt-Pt} with increase of the Ce loading was less pronounced than observed for the $yCexPtAl\_Cl$ samples, since the Cl-free series without Ce presented lower N_{Pt-Pt} of 4.0, indicating that all the Pt atoms were at the surface [59].

In general, the increase in the degree of oxidation with ceria loading, indicated by the N_{Pt-O} values obtained from the EXAFS analysis, was also observed by linear combination analysis (LCA) of the XANES data. The distributions of the Pt^0 and Pt-O species are shown in Table S5. The degree of oxidation is related to the white-line intensity, which increased with increase of the Ce content. This was confirmed by the LCA, with decreasing percentages of metallic platinum of 96.2 %, 90.3 %, and 88.2 %Pt^0 for the 1PtAl_Cl, 3Ce1PtAl_Cl, and 6Ce1PtAl_Cl samples, respectively. Similar decreasing percentages were observed for the non-chlorinated samples, with values of 78.3 %, 72.5 %, and 66.5 %Pt^0 for the 1PtAl, 3Ce1PtAl, and 6Ce1PtAl catalysts, respectively.

Table 3

LCA of XANES spectra at the Ce L$_3$-edge for the 6Ce03PtAl, 6Ce03PtAl_Cl, 6Ce2PtAl, and 6Ce2PtAl_Cl samples, calcined (fresh) and after reduction (at 500 °C, under a flow of H_2).

Condition	Sample (chlorinated)	Ce^{3+} %	Ce^{4+} %	Sample (non-chlorinated)	Ce^{3+} %	Ce^{4+} %
Calcined	6Ce03PtAl_Cl	0	100	6Ce03PtAl	0	100
	6Ce2PtAl_Cl	2	98	6Ce2PtAl	1	99
Reduced	6Ce03PtAl_Cl	41	59	6Ce03PtAl	65	35
	6Ce2PtAl_Cl	71	29	6Ce2PtAl	66	34

STEM analyses were also used to determine the mean Pt particle diameters for the samples with ceria promotion (Table 1 and Table 2). The images are provided in Fig. S8. Despite the low contrast between the Pt and ceria particles, the estimated sizes suggested a decrease in the mean Pt particle diameter with increase of the Ce loading, in agreement with the EXAFS results, where D_{Pt} was estimated based on the N_{Pt-Pt} parameter (Table 1 and Table 2). The particle diameters determined from the STEM images were 1.4, 1.0, and 1.1 nm for 2PtAl_Cl, 3Ce2PtAl_Cl, and 6Ce2PtAl_Cl, respectively, while the diameters for the Cl-free samples were 1.2 and 1.0 nm for the 2PtAl and 6Ce2PtAl catalysts, respectively. The diameters obtained for the $yCexPtAl$ samples using the EXAFS model were slightly smaller than estimated by STEM (for example, 0.74 nm for the 6Ce2PtAl sample). The low Pt-Pt coordination of the first shell with high oxygen coverage of the samples (N_{Pt-O} higher than 1.4) suggested that the ceria loading altered the morphology of the particles, with flattening of spherical nanoparticles with high surface curvature, involving interaction with oxygen [60].

3.2. Electronic effect of Ce addition in Pt/Al$_2$O$_3$ catalysts

The CO-FTIR results, as discussed previously for the samples without Ce promotion [3], indicated the absence of bands corresponding to oxidized species (Pt^{n+}, 1 <n< 2), [50] which could be explained by inaccessibility of the Pt-CO bond [61] or by oxidation of CO to CO_2 [62]. However, it is possible that in the presence of ceria, the reactivity of oxygen with Pt changed the local electron density of the Pt surface, [63] due to the creation of more positively charged Pt species, such as Pt$^{\delta+}$ (1 >δ) [50]. Therefore, as reported for Pt supported on Al$_2$O$_3$, [3] the catalysts promoted with ceria could be represented by a structural model with particles composed by Pt^0 sites in the core, with oxygen at the surface, suggesting interaction with the support and/or the ceria. Consequently, the Pt-Pt and Pt-O bond lengths (R_{Pt-Pt} and R_{Pt-O}) reflected the electron density of Pt sites in the core and at the surface, [3] respectively. This structure suggested a reconfiguration of the Pt and O atoms, where PtO interacted with the Pt^0 core, creating a disordered Pt-O-Ce-O-Pt layer. Both morphological changes and the interaction of Pt with oxygen could contribute to decrease of N_{Pt-Pt}, similar to the behavior observed for Cu nanoparticles under N_2O oxidation conditions [2].

The Pt-Pt and Pt-O bond lengths (R_{Pt-Pt} and R_{Pt-O}) obtained by EXAFS are also shown in Tables 1 and 2. For the Cl-containing samples, the Pt-Pt distance decreased slightly with increase of the ceria loading, as illustrated by values of 2.75 ± 0.001 Å for 03PtAl_Cl and 2.74 ± 0.004 Å for 6Ce03PtAl_Cl, while the Pt-Pt bond length for a bulk Pt^0 standard is 2.77 ± 0.004 Å. Shortening of the Pt-Pt bond is related to decrease of the Pt particle size, [64] although greater contraction (0.1 Å) was expected, compared to the bulk material [64]. For the Cl-free samples, the Pt-Pt bond distance did not change with Ce loading, with the $yCe03PtAl$ and $yCe1PtAl$ catalysts showing a value of around 2.75 ± 0.01 Å. This suggested that the contraction caused by the size decrease (the N_{Pt-Pt} values were 4.51 ± 0.31 for 1PtAl and 3.60 ± 0.07

for 6Ce1PtAl) was compensated by relaxation upon interaction with oxygen [65] (with N_{Pt-O} values of 1.67 ± 0.12 for 1PtAl and 2.16 ± 0.22 for 6Ce1PtAl), resulting in a similar surface Pt electron density. In previous work, EXAFS results indicated a relaxation of R_{Cu-O} for a Ce-promoted catalyst, compared to unpromoted Cu nanoparticles (around 1 nm in size), with the bond length expansion decreasing with ceria loading [2]. In contrast, in this work, besides the differences in N_{Pt-Pt} and N_{Pt-O}, the addition of Ce to the PtAl samples did not change the R_{Pt-O} distance (within the parameter uncertainty). For example, the values were 2.02 ± 0.02 for 1PtAl_Cl and 2.01 ± 0.01 for 6Ce1PtAl_Cl, while the values for the Cl-free samples were 2.01 ± 0.01 for 1PtAl and 6Ce1PtAl. This similarity of the Pt-O bond length for different N_{Pt-Pt} and N_{Pt-O} indicated insensitivity of the electron density of surface platinum nanoparticles to the Ce promotion.

To better understand the promotion of Pt nanoparticles by ceria, it is important to investigate the degree of reduction of the Ce species. The XANES analysis at the Ce L_3-edge for the Cl-containing and Cl-free 6Ce03PtAl and 6Ce2PtAl samples showed the distributions of cerium species (Ce^{3+} and Ce^{4+}) after calcination and after reduction (Table 3). The Ce L_3-spectra of the reduced samples are shown in Fig. 3. The calcined samples showed the presence of cerium oxide (CeO_2) species (not shown). After in situ H_2 treatment at 500 °C, Ce^{4+} was partially reduced to Ce^{3+}, as suggested in the TPR experiments by the higher H_2 uptake below 500 °C, compared to the PtAl samples (Table S3). The amount of Ce^{3+} species was about 65 % for the Cl-free samples, while for the chlorinated catalysts, the amount increased with Pt loading (41 % for 6Ce03PtAl_Cl and 71 % for 6Ce2PtAl_Cl). The presence of Ce^{3+} species, or vacancy formation (O_{vac}), could be correlated to the size of the Ce nanoparticles, [66] and to the Pt-ceria interaction through the Pt-O-Ce bond. However, the XRD results (Table S3) indicated similar larger CeO_2 crystal size for each series (Cl-containing and Cl-free samples), with the same size of the crystallites (7 nm, Table S3), which were outside the pores, suggesting that the vacancies formation/degree of ceria reduction could be correlated with the Ce nanoparticle size [66]. For the yCexPtAl_Cl samples, the increased degree of reduction with Pt loading could be due to the presence of residual chloride, which improved the reducibility of ceria, [67] as suggested by the TPR results. However, the effect of chloride on oxygen storage capacity (OSC) in ceria-based catalysts is strongly dependent on the degree of chlorination of Pt, which could lead to redispersion of Pt and improvement of OSC after oxychlorination treatments [68,69]. It is also possible that the exchange of some lattice O^{2-} with Cl^- ions on the ceria surface led to the formation of CeOCl [70] or $Ce(OH)_2Cl$ species, blocking the oxygen vacancies and stabilizing the Ce^{3+} species [71]. As the chlorine content increased with the Pt loading, it could lead to an increasing amount of

these soluble species, increasing the amount of Ce^{3+}. Therefore, for the Cl-containing samples, the degree of reduction of the ceria did not reflect the capacity for storage/release of oxygen, since the chlorine could stabilize and hinder the Ce^{3+}/Ce^{4+} interconversion, consequently affecting the redox properties of the ceria.

3.3. Effect of Ce promotion on WGSR activity

Fig. S7 shows the in situ DRIFTS spectra acquired under WGSR conditions at 200–350 °C for the unpromoted catalyst (03PtAl_Cl) and the catalyst promoted with ceria (6Ce03PtAl_Cl). The 03PtAl_Cl sample presented a main band at 2067 cm^{-1}, with a small shoulder at 2038 cm^{-1}, while the 6Ce03PtAl_Cl sample presented a main band at 2051 cm^{-1}, with high frequency (2074 cm^{-1}) and low frequency (2018 cm^{-1}) shoulders, indicating Pt^0 sites linearly bonding CO [47]. Bands characteristic of monodentate formate (m-HCOO) were observed for υ_{C-H} at 3000 cm^{-1}, $\upsilon_{as\ OCO}+ \delta_{CH}$ at 2910 cm^{-1}, and $\upsilon_{as\ OCO}$ at 1590 cm^{-1} [72,73]. A band characteristic of carboxylate ($\upsilon_{as\ OCO}$ $CO_2^{\delta-}$) occurred at 1650 cm^{-1}. As previously demonstrated by c-MES (modulation excitation spectroscopy), the m-HCOO and carboxylate ($CO_2^{\delta-}$) species, probably located at the metal-support interface, were reaction intermediates [74] However, Kalamaras et al. [75] observed that for the WGS at 300 °C, the specific reaction rate increased linearly with Pt particle size between 1.3 and 8 nm, which was associated with steady-state isotopic transient kinetic results, suggesting that the reaction proceeded mainly according to the redox mechanism at sites located at the periphery of the Pt–CeO$_2$ interface. The adsorption of water was favored on Pt-O-Ce vacancy sites, compared to Pt clusters, by 0.70 eV. This was consistent with the observed higher activity for samples with high levels of Pt-O species that could interact with the ceria and create Pt-O-Ce active sites, which could allow the redox mechanism with reversible changes of Pt^0↔Pt^{2+} and Ce^{3+}↔Ce^{4+} [76].

In order to investigate the effects of the structural parameters on the activities of the yCexPtAl and yCexPtAl_Cl catalysts in the WGSR, the forward turnover frequency (TOF$_f$) was calculated using the CO conversion at 300 °C, with P_{CO} and P_{H_2O} of 0.05 and 0.15 atm, respectively, considering the density of Pt^0 sites quantified by CO-FTIR as the active sites (Table S6). Fig. 4 shows the TOF$_f$, according to Pt loading, for the yCexPtAl_Cl and yCexPtAl samples with different ceria loadings. The addition of Ce to the Cl-free catalysts improved the activity by around 2–10 times, compared to the unpromoted catalysts, which was higher than when Ce was added to the chlorine-containing catalysts. An apparent correlation of TOF$_f$ with Ce/Pt was observed (Table S6). However, as demonstrated previously, [68,69] the interaction of Cl with CeO_2 could modify the oxy-reduction properties of the ceria, so in the case of the Cl-containing samples, only the Cl-free ceria fraction should be considered, as (Ce-Cl)/Pt, for correlation with activity.

As shown in Fig. 5, the TOF$_{forw}$ was correlated with N_{Pt-O}/N_{Pt-Pt} for the yCexPtAl and yCexPtAl_Cl catalyst series. The Pt-Pt coordination number (N_{Pt-Pt}) decreased with Ce loading, while the Pt-O coordination number (N_{Pt-O}) increased, indicating greater contact with the ceria. It has been reported that decrease of the Pt particle size leads to greater contact with ceria, modifying the electronic properties, with the platinum density enhancing water activation [77]. However, although the addition of ceria led to changes in the N_{Pt-Pt-} and N_{Pt-O} coordination numbers, there was no difference in the global nanoparticle electron density, since the Pt-O bond distances were almost the same (2.01 ± 0.01). The small changes of the surface electronic properties were evidenced from the position of the band for adsorbed CO (Fig. 2). This means that the electronic density of the Pt surface was not the main factor governing the WGSR activity for the Ce-containing samples. It is reasonable to suggest the emergence of new catalytic sites with different natures, such as interfacial sites composed by a CeO$_x$ domain around the Pt clusters [78]. There was a dependence of activity (TOF$_f$) on the Ce/Pt bulk ratio, suggesting a key role of ceria at the interface with platinum in lowering the energy barrier of the WGSR rate determining step, by
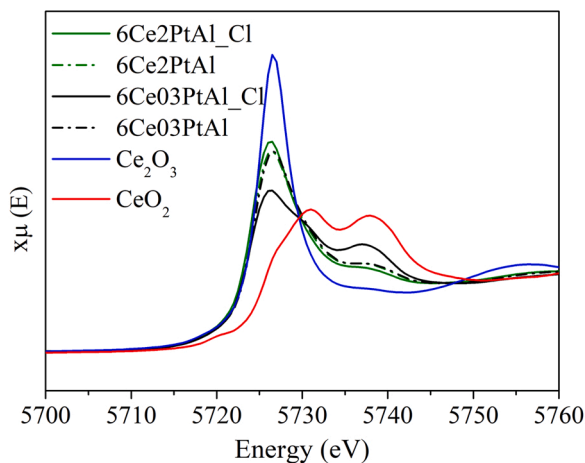

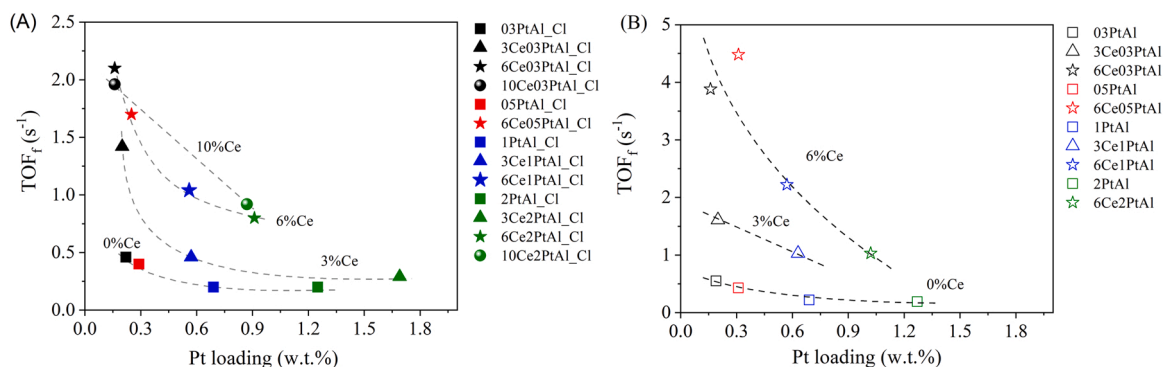**Fig. 3.** XANES spectra at the Ce L_3-edge for the reduced 6CexPtAl _Cl and 6CexPtAl samples.

Fig. 4. Forward turnover frequency (TOF$_f$) at 300 °C *versus* Pt loading, obtained by XRF, for the *yCexPtAl_Cl* (A) and *yCexPtAl* (B) samples.
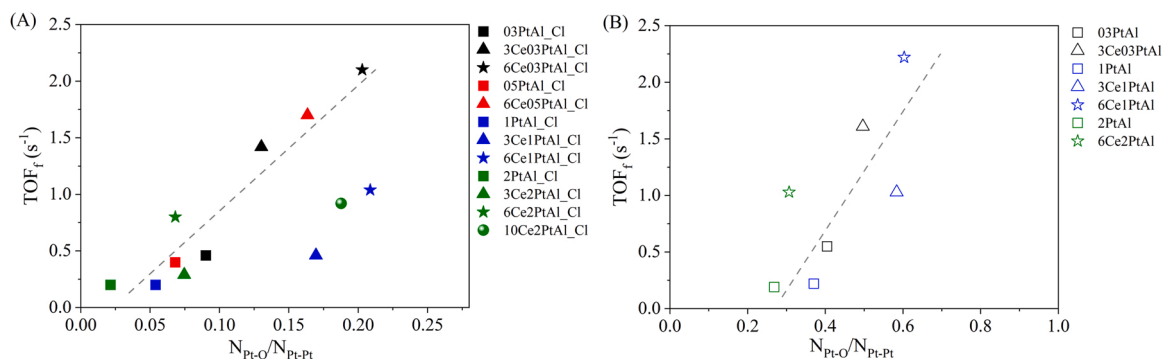

Fig. 5. Forward turnover frequency (TOF$_f$) at 300 °C *versus* the ratio of Pt-O coordination number (N$_{Pt-O}$) to Pt-Pt coordination number (N$_{Pt-Pt}$), for the *yCexPtAl_Cl* (A) and *yCexPtAl* (B) samples.

means of Pt-O-Ce interaction. The promoting effect of ceria in the Cl-free samples could also suggest an effective Pt-O-Ce interaction, leading to high activity in the WGSR. The same Ce/Pt ratio for 3Ce1PtAl and 6Ce2PtAl, together with the same TOF$_f$ (1.03 s^{-1}), provided further evidence of the importance of the Ce domain around the Pt^0 sites in determining the activity.

Therefore, since the addition of ceria led to an increase in activity of around 2–10 times, compared to the unpromoted system, this indicated that the reaction did not occur exclusively at the Pt^0 surface, but rather at the Pt-O-Ce interface, suggesting alteration of the WGSR pathways.

Hence, there was a correlation between the structural properties of the Pt nanoparticles and the presence of ceria. The presence of ceria, the Pt loading, and the preparation method determined the structural parameters (N$_{Pt-O}$ and N$_{Pt-O}$), which influenced the surface structure by means of the Pt-O-Ce interaction, consequently affecting the catalytic activity. Therefore, considering a bifunctional catalyst, the reaction rate would provide a better estimate of the activity of the system. The forward WGS reaction rate (R$_f$) was calculated based on the amount of catalyst (μmol$_{CO}$.s^{-1}.g$_{cat}^{-1}$) and the metal content (μmol$_{CO}$.s^{-1}.g$_{Pt}^{-1}$) (Table S6). Subtraction of the value of R for the corresponding Ce-free sample then provided a reaction rate related to the Ce content (r$_{Ce}$). In opposition to the TOF$_f$ values (Table S6), the overall apparent rate of reaction for CO consumption (μmol$_{CO}$.s^{-1}.g$_{cat}^{-1}$) and the apparent rate for ceria (r$_{Ce}$) increased with Pt loading, indicating that the activity was related to the presence of a Pt-O-Ce interface that changed the rate limiting step of the reaction.

In opposition to the TOF values, the apparent rates for the Cl-free samples were higher than for the Cl-containing samples, indicating a poisoning effect of Cl$^-$ remaining on the interfacial sites. Nevertheless, the r$_{Ce}$ values for the Cl-free samples were lower than for the Cl-containing samples. Since the surface sites were not poisoned by Cl$^-$, the overall activity could have been better distributed at the Pt-O-Ce

interface, compared to the Cl-containing samples where Ce appeared to have a greater role in the activity, at the expense of Pt.

3.4. Role of Pt-O-Ce interface sites in WGSR activity

Considering that the Pt-O-Ce sites at the Pt-ceria interface were the main active sites, the forward reaction rate for CO consumption (R$_f$, in μmol$_{CO}$.s^{-1}.g$_{Pt}^{-1}$) was correlated using a factor proportional to Pt on the nanoparticle surface in interaction with ceria, denoted here by f(Pt-O-Ce)$_s$. For calculation of this factor, the fraction of Pt^0 on the nanoparticle surface (f(Pt)$_s$) was firstly estimated: i) The catalysts were divided into two series, depending on the N$_{Pt}$ coordination number; ii) For Pt nanoparticles with N$_{Pt-Pt}$ lower than 4.6, it was considered that all the Pt atoms were exposed on the surfaces of the nanoparticles (f(Pt)$_s$ = 1); iii) In the case of the *yCexPtAl_Cl* catalyst series with N$_{Pt-Pt}$ higher than 4.6, f(Pt)$_s$ was calculated using the correlation obtained previously, [79] where f(Pt)$_s$ = 1.925-(0.15 N$_{Pt-Pt}$). The ceria content that did not interact with Cl, relative to Pt, was calculated using the ratio [Ce – (Cl 140.11/35.5)]/Pt. Finally, f(Pt-O-Ce)$_s$ was calculated from f(Pt)$_s$ times the ratio [Ce – (Cl 140.11/35.5)], divided by the Pt content, where f(Pt-O-Ce)$_s$ = f(Pt)$_s$ N$_{Pt-O}$[(Ce-(Cl 140.11/35.5)]/Pt. Here, f(Pt-O-Ce)$_s$ is the probability factor for finding the Pt atom on the surface neighboring Pt-O, which in turn interacts with ceria free of Cl to form the Pt-O-Ce site. The reaction rate for CO consumption per platinum at the surface was estimated (R$_f$.f(Pt)$_s$) and denoted as R$_{fs}$ (μmol$_{CO}$.s^{-1}.g$_{Pts}^{-1}$). The correlation between the reaction rate for CO consumption (R$_{fs}$) and the factor f(Pt-O-Ce)$_s$ is shown in Fig. 6.

The PtAl samples where f(Pt-O-Ce)$_s$ = 0 (Fig. 6) showed high dispersion of the activity values, between 452 and 1410 μmol$_{CO}$.s^{-1}.g$_{Pt}^{-1}$. As demonstrated previously for PtAl and PtAl_Cl catalysts, [3] as the Pt loading was increased, adsorbed CO strongly blocked the active sites, decreasing the access of reactants to the Pt active sites. Interestingly,
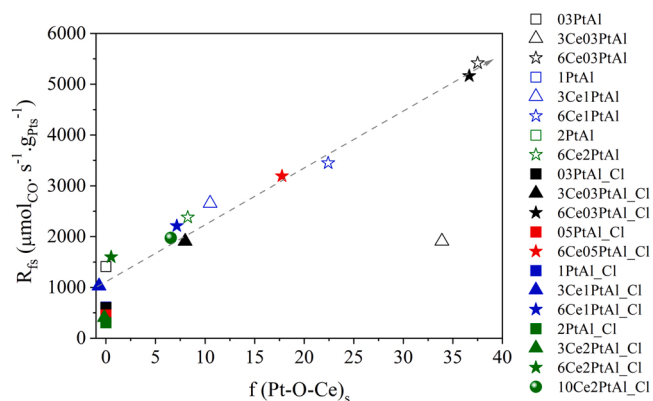
Fig. 6. Forward reaction rate at the surface (R_{fs}) for CO conversion (μmol_{CO}. $s^{-1}.g_{Pt}^{-1}$) according to the fraction of Pt-O-Ce ($f(Pt\text{-}O\text{-}Ce)_s$).

with addition of ceria, the reaction rate became directly proportional to the factor f(Pt-O-Ce), which was proportional to the Pt-O-Ce interface. These results suggested that the slight changes in electronic density on the Pt surface (detected from the adsorbed CO) were irrelevant. This indicated that control of the reaction rate became related to the presence of Pt-O-Ce sites.

The Pt nanoparticles supported on Al_2O_3, as described in previous work, [3] presented a core-shell type structure, formed by a core of Pt^0 with $Pt\text{-}O_x$ on the surface. The EXAFS spectra indicated that lower $N_{Pt\text{-}Pt}$ was associated with higher $N_{Pt\text{-}O}$, which were correlated (Fig. S10) and determined the surface structures of the Pt nanoparticles interacting with oxygen. However, the bond distances ($R_{Pt\text{-}O}$ and $R_{Pt\text{-}Pt}$) were identical for different coordination numbers, indicating the existence of compensation between the electronic effect of the size of the Pt^0 core and the density of Pt-O species on the surface. The addition of ceria to xPtAl and xPtAl_Cl led to a smaller Pt particle size and higher oxygen coverage, suggesting that ceria interacted with platinum by means of surface oxygen, according to Pt-O-Ce interactions, which could be hindered by remaining Cl in the yCexPtAl_Cl samples. However, with addition of ceria, there was decrease of $N_{Pt\text{-}Pt}$ and increase of $N_{Pt\text{-}O}$, indicating that sintering of the Pt nanoparticles was reduced by the presence of ceria, due to decreased diffusion of Pt at the surface of the Ce-containing support. Similar values for the $R_{Pt\text{-}O}$ and $R_{Pt\text{-}Pt}$ bond distances suggested similar global surface electronic properties for the different PtAl and PtCeAl catalysts ($R_{Pt\text{-}O}$ = 2.00–2.01 Å). Improvements of TOF between around 2 and 10 times were achieved, compared to Pt on alumina surfaces, described in the literature [11,18,77]. This improvement was related to the generation of oxygen vacancies on the ceria close to platinum, which were fundamental for water dissociation during the WGSR, [19,22] commonly acknowledged to be a rate-limiting step [19,22]. Bruix et al. [77] reported that strong metal-support interaction was responsible for marked electronic perturbations for small particles of platinum in contact with ceria, which significantly enhanced the dissociation of water on the Pt. However, the theoretical model for Pt nanoparticles considers the interaction Pt-O-supported metal, without consideration of the Pt-O on the surface. The $R_{Pt\text{-}Pt}$ and $R_{Pt\text{-}O}$ bond lengths were similar for various samples, and the EXAFS results indicated that there was no electronic modification at the Pt surface. The FTIR results showed slight changes of the band position for linearly adsorbed CO, together with the presence of CO species adsorbed in bridge form on the unpromoted catalyst. For the unpromoted PtAl catalysts, increase of the Pt loading led to adsorbed CO strongly blocking the active sites, decreasing the accessibility of reactive Pt sites [3]. This effect resulted in changes in activity, such as TOF values from 0.20 to 0.46 s^{-1} (452–850 $\mu mol_{CO}.s^{-1}.g_{Pt}^{-1}$). Interestingly, with addition of ceria, the reaction rate changed from 0.29 to 1.96 s^{-1} (1410–5000 $\mu mol_{CO}.s^{-1}.g_{Pt}^{-1}$). These activity values were directly proportional to the factor $f(Pt\text{-}O\text{-}Ce)_s$, which was proportional to the

Pt-O-Ce interface.

The EXAFS analysis showed similar $R_{Pt\text{-}Pt}$ and $R_{Pt\text{-}O}$ bond length values for different $N_{Pt\text{-}Pt}$ between 3.8 and 8.4, indicating that the influence of confinement effects on the electronic properties was irrelevant. The position of the band for adsorbed CO showed slight changes, while the band corresponding to linearly bonded CO was in similar regions for the promoted and unpromoted catalysts. Therefore, the higher activity observed for the Ce-containing catalysts could be not explained by slight changes in the electronic properties of the samples. Hence, the improvement in activity was due to the creation of interfacial sites, resulting in the activation and dissociation of water at interfacial oxygen vacancies (O-H bonds), [80] with stabilized intermediates such as –COOH and –CO2 [11]. The microkinetic model showed the importance of neighboring surface –OH groups in facilitating water dissociation at the metal-oxide interface [80]. The number density of active sites (Pt-O-Ce) was correlated to the periphery of the Pt-Ce interface, [19] for water dissociation. The smaller heat of CO adsorption for Pt sites at the Pt-Ce interface, as discussed in the literature, [21,81] could increase the reactivity of the CO in the presence of the Pt-O-Ce interaction. The correlation of yCexPtAl_Cl and yCexPtAl activity with Pt-O-Ce interfacial sites ($f_{Pt\text{-}Ce}$), which are formed on the surface of Pt nanoparticles, demonstrated the importance of Ce domains for enhancing the activity, such as by improving water dissociation at interfacial oxygen vacancies. The stabilization of vacancy structure by the presence of Cl in the yCexPtAl_Cl samples could increase the activation barrier to water dissociation, leading to a decrease of the WGS reaction rate. The findings showed the importance of the reversible interconversion of $Ce^{4+}/Ce^{3+}\text{-}O_v$ species [82] available to form species such as H/OH at a dynamic surface, which is not connected with structural properties of the ceria.

4. Conclusions

The addition of ceria to PtO_2/Al_2O_3 samples modified the Pt particle size in the resulting catalysts. The Pt particle size decreased with increase of the ceria loading, with correlation observed between structural parameters such as the coordination numbers at the first coordination shell ($N_{Pt\text{-}Pt}$ and $N_{Pt\text{-}O}$). The decrease of Pt size with $N_{Pt\text{-}Pt}$ led to increase of $N_{Pt\text{-}O}$, suggesting that the degree of oxygen coverage depended on the Pt particle size and increased with decrease of the Pt particle size.

A model for the Pt nanoparticles was proposed, based on a Pt^0 core and a shell of Pt-oxygen, with part of the oxygen being on the Pt core surface (Pt-O) and another part being in interaction at the interface with the alumina support (Pt-O-Al). For the non-chlorinated PtO_2/Al_2O_3 catalysts, this effect of Pt dispersion due to the presence of ceria was not intense. The distinct behavior of the Cl-free samples could be attributed to a higher $N_{Pt\text{-}O}/N_{Pt\text{-}Pt}$ ratio, indicating different morphologies of the chlorinated and non-chlorinated sample series. The increase of $N_{Pt\text{-}O}/N_{Pt\text{-}Pt}$ in the presence of ceria suggested the establishment of interaction with ceria (Pt-O-Ce) at the interface. With the addition of ceria, part of the local $Pt_x\text{-}O$ structure in the Ce-free catalysts was modified to $Pt_x\text{-}(O\text{-}Ce)_2$, increasing the Pt-O scattering.

Contraction of the Pt−Pt bond lengths ($R_{Pt−Pt}$), due to the confinement effect, was not observed with decrease of $N_{Pt\text{-}Pt}$. Overall, the electronic densities were similar for the Pt nanoparticles with different sizes. This could be explained by interaction with oxygen at the surface. The decrease of the Pt nanoparticle size would be expected to increase the electronic density and the reactivity with oxygen.

The presence of PtO on the surface resulted in a compensation effect between Pt core size and oxygen coverage. Consequently, the samples with different $N_{Pt\text{-}Pt}$ and $N_{Pt\text{-}O}$, with or without the presence of ceria, showed similar bond lengths for Pt-O ($R_{Pt\text{-}O}$), at around 2.00 Å, and for Pt-Pt ($R_{Pt\text{-}Pt}$), at around 2.74 Å, revealing similar electronic density of Pt^0 in the various Pt nanoparticle catalysts.

In terms of activity in the WGSR, based on Pt^0 surface sites, the addition of ceria led to improvement of TOF by between 2 and 10 times,

compared to the unpromoted samples, which was not related to the electronic properties of the Pt nanoparticle surface, since they did not change significantly. The reaction rate ($\mu mol_{CO}.s^{-1}.g_{Pt}^{-1}$) was correlated with a factor proportional to the density of Pt-O-Ce sites, which, associated with higher activity, suggested that the pathway of the WGSR and the rate determining step were modified by the presence of ceria interacting at the surface by means of Pt-O-Ce interface sites. The lower promotion provided by the ceria in the Cl-containing catalysts suggested that the remaining chlorine affected the ceria mobility, hindering the Ce^{3+}/Ce^{4+} interconversion and the effectiveness at the Pt-O-Ce interface.

Declaration of Competing Interest

The authors declare that they have no known competing financial interests or personal relationships that could have appeared to influence the work reported in this paper.

Data Availability

No data was used for the research described in the article.

Acknowledgments

Appendix A. Supporting information

Supplementary data associated with this article can be found in the online version at doi:10.1016/j.apcatb.2023.122361.

References

[1] C.N. Ávila-Neto, D. Zanchet, C.E. Hori, R.U. Ribeiro, J.M.C. Bueno, Interplay between particle size, composition, and structure of MgAl 2O4-supported Co-Cu catalysts and their influence on carbon accumulation during steam reforming of ethanol, J. Catal. 307 (2013) 222–237, https://doi.org/10.1016/j.jcat.2013.07.025.

[2] P.C.P. Caldas, J.M.R. Gallo, A. Lopez-castillo, D. Zanchet, J.M.C. Bueno, The structure of the Cu − CuO sites determines the catalytic activity of Cu nanoparticles, ACS Catal. 7 (2017) 2419–2424, https://doi.org/10.1021/acscatal.6b03642.

[3] L.R. Borges, A. Lopez-Castillo, D.M. Meira, J.M.R. Gallo, D. Zanchet, J.M.C. Bueno, Effect of the Pt precursor and loading on the structural parameters and catalytic properties of Pt/Al2O3, ChemCatChem 11 (13) (2019) 3064–3074, https://doi.org/10.1002/cctc.201900092.

[4] D.M. Meira, R.U. Ribeiro, O. Mathon, S. Pascarelli, J.M.C. Bueno, D. Zanchet, Complex interplay of structural and surface properties of ceria on platinum supported catalyst under water gas shift reaction, Appl. Catal. B Environ. 197 (2016) 73–85, https://doi.org/10.1016/j.apcatb.2016.04.025.

[5] K. An, S. Alayoglu, N. Musselwhite, S. Plamthottam, A.E. Lindeman, G.A. Somorjai, Enhanced CO oxidation rates at the interface of mesoporous oxides and Pt nanoparticles, J. Am. Chem. Soc. 135 (2013) 16689–16696, https://doi.org/10.1021/ja4088743.

[6] C. Song, Fuel processing for low-temperature and high-temperature fuel cells challenges, and opportunities for sustainable development in the 21st century, Catal. Today 77 (2002) 17–49, https://doi.org/10.1016/S0920-5861(02)00231-6.

[7] D.W. Flaherty, W.-Y. Yu, Z.D. Pozun, G. Henkelman, C.B. Mullins, Mechanism for the water–gas shift reaction on monofunctional platinum and cause of catalyst deactivation, J. Catal. 282 (2) (2011) 278–288, https://doi.org/10.1016/j.jcat.2011.06.024.

[8] S.C. Ammal, A. Heyden, Water-gas shift catalysis at corner atoms of Pt clusters in contact with a TiO2 (110) support surface, ACS Catal. 4 (10) (2014) 3654–3662, https://doi.org/10.1021/cs5009706.

[9] K.C. Petallidou, K. Polychronopoulou, S. Boghosian, S. Garcia-rodriguez, A. M. Efstathiou, Water − gas shift reaction on Pt / Ce 1−x Ti x O2 − Δ: the effect of Ce/Ti ratio, J. Phys. Chem. C 48 (118) (2013) 25467–25477, https://doi.org/10.1021/jp406059h.

[10] E.A. Walker, D. Mitchell, G.A. Terejanu, A. Heyden, Identifying active sites of the water-gas shift reaction over titania supported platinum catalysts under

[11] S. Aranifard, S.C. Ammal, A.H. Heyden, On the importance of metal-oxide interface sites for the water-gas shift reaction over Pt/CeO2 catalysts, J. Catal. 309 (2014) 314–324, https://doi.org/10.1016/j.jcat.2013.10.012.

[12] Y. Li, Q. Fu, M. Flytzani-Stephanopoulos, Low-temperature water-gas shift reaction over Cu- and Ni-loaded cerium oxide catalysts, Appl. Catal. B Environ. 27 (3) (2000) 179–191, https://doi.org/10.1016/S0926-3373(00)00147-8.

[13] J. Ke, W. Zhu, Y. Jiang, R. Si, Y.-J. Wang, S.-C. Li, C. Jin, H. Liu, W.-G. Song, C.-H. Yan, Y.-W. Zhang, Strong local coordination structure effects on subnanometer PtO x Clusters over CeO 2 nanowires probed by low-temperature CO oxidation, ACS Catal. 5 (9) (2015) 5164–5173, https://doi.org/10.1021/acscatal.5b00832.

[14] L.R. Borges, A.G.M. Silva, A.H. Braga, L.M. Rossi, M.A. Suller Garcia, P. Vidinha, Cover feature: towards the effect of Pt 0 /Pt Δ+ and Ce 3+ species at the surface of CeO 2 crystals: understanding the nature of the interactions under CO oxidation conditions, ChemCatChem 13 (5) (2021), https://doi.org/10.1002/cctc.202100172, 1249–1249.

[15] Y. Nagai, T. Hirabayashi, K. Dohmae, N. Takagi, T. Minami, H. Shinjoh, S. Matsumoto, Sintering inhibition mechanism of platinum supported on ceria-based oxide and Pt-oxide-support interaction, J. Catal. 242 (1) (2006) 103–109, https://doi.org/10.1016/j.jcat.2006.06.002.

[16] H. Shinjoh, M. Hatanaka, Y. Nagai, T. Tanabe, N. Takahashi, T. Yoshida, Y. Miyake, Suppression of noble metal sintering based on the support anchoring effect and its application in automotive three-way catalysis, Top. Catal. 52 (13–20) (2009) 1967–1971, https://doi.org/10.1007/s11244-009-9371-5.

[17] Y. Zhou, J.M. Perket, J. Zhou, Growth of Pt nanoparticles on reducible CeO2(111) thin films: effect of nanostructures and redox properties of ceria, J. Phys. Chem. C. 114 (27) (2010) 11853–11860, https://doi.org/10.1021/jp1007279.

[18] A. a Phatak, N. Koryabkina, S. Rai, J.L. Ratts, W. Ruettinger, R.J. Farrauto, G. E. Blau, W.N. Delgass, F.H. Ribeiro, Kinetics of the water–gas shift reaction on Pt catalysts supported on alumina and ceria, Catal. Today 123 (1–4) (2007) 224–234, https://doi.org/10.1016/j.cattod.2007.02.031.

[19] C.M. Kalamaras, S. Americanou, A.M. Efstathiou, '" Redox "' vs '" associative formate with – OH Group Regeneration "' WGS reaction mechanism on Pt / CeO 2: effect of platinum particle size, J. Catal. 279 (2011) 287–300, https://doi.org/10.1016/j.jcat.2011.01.024.

[20] C.M. Kalamaras, I.D. Gonzalez, R.M. Navarro, J.L.G. Fierro, A.M. Efstathiou, Effects of reaction temperature and support composition on the mechanism of water - gas shift reaction over supported-Pt catalysts, J. Phys. Chem. C 115 (23) (2011) 11595–11610, https://doi.org/10.1021/jp201773a.

[21] D.M. Meira, R.U. Ribeiro, O. Mathon, S. Pascarelli, J.M.C. Bueno, D. Zanchet, Complex interplay of structural and surface properties of ceria on platinum supported catalyst under water gas shift reaction, Appl. Catal. B Environ. 197 (2016) 73–85, https://doi.org/10.1016/j.apcatb.2016.04.025.

[22] J.A. Rodriguez, P. Liu, J. Hrbek, J. Evans, M. Pérez, Water gas shift reaction on Cu and Au nanoparticles supported on CeO 2(111) and ZnO(0001): intrinsic activity and importance of support interactions, Angew. Chem. - Int. Ed. 46 (8) (2007) 1329–1332, https://doi.org/10.1002/anie.200603931.

[23] A.A. Gokhale, J.A. Dumesic, M. Mavrikakis, On the mechanism of low-temperature water gas shift reaction on copper on the mechanism of low-temperature water gas shift reaction on copper, J. Am. Chem. Soc. 130 (33) (2008) 1402–1414, https://doi.org/10.1021/ja0768237.

[24] J.A. Rodriguez, J. Graciani, J. Evans, J.B. Park, F. Yang, D. Stacchiola, S. D. Senanayake, S. Ma, M. Perez, P. Liu, J.F. Sanz, J. Hrbek, Water-gas shift reaction on a highly active inverse CeO, x/Cu(111) catalyst: unique role of ceria nanoparticles, Angew. Chem. - Int. Ed. 48 (43) (2009) 8047–8050, https://doi.org/10.1002/anie.200903918.

[25] J.M. Zalc, V. Sokolovskii, D.G. Löffler, Are noble metal-based water–gas shift catalysts practical for automotive fuel processing? J. Catal. 206 (2002) 169–171, https://doi.org/10.1006/jcat.2001.3465.

[26] Q. Fu, H. Saltsburg, M. Flytzani-Stephanopoulos, Active nonmetallic Au and Pt species on ceria-based water-gas shift catalysts, Science 301 (5635) (2003) 935–938, https://doi.org/10.1126/science.1085721.

[27] A.M. Gänzler, M. Casapu, F. Maurer, H. Störmer, D. Gerthsen, G. Ferré, P. Vernoux, B. Bornmann, R. Frahm, V. Murzin, M. Nachtegaal, M. Votsmeier, J.D. Grunwaldt, Tuning the Pt/CeO2 interface by in situ variation of the Pt particle size, ACS Catal. 8 (6) (2018) 4800–4811, https://doi.org/10.1021/acscatal.8b00330.

[28] M. Cargnello, V.V.T. Doan-Nguyen, T.R. Gordon, R.E. Diaz, E. a Stach, R.J. Gorte, P. Fornasiero, C.B. Murray, Control of metal nanocrystal size reveals metal-support interface role, Sciences (80-.) 341 (6147) (2013) 771–773, https://doi.org/10.1126/science.1240148.

[29] X. Lai, D.W. Goodman, Structure-reactivity correlations for oxide-supported metal catalysts: new perspectives from STM, J. Mol. Catal. A Chem. 162 (2000) 33–50, https://doi.org/10.1016/S1381-1169(00)00320-4.

[30] R. Tiwari, B. Sarkar, R. Tiwari, C. Pendem, T. Sasaki, R. Saran, R. Bal, Pt nanoparticles with tuneable size supported on nanocrystalline ceria for the low temperature water-gas-shift (WGS) reaction, J. Mol. Catal. A Chem. 395 (2014) 117–123, https://doi.org/10.1016/j.molcata.2014.08.021.

[31] A. Vazquez, T. Lopez, R. Gomez, X. Bokhimi, Synthesis, characterization and catalytic properties of Pt / CeO2 – Al2O3 and Pt/La2O3 – Al2O3 sol – gel derived catalysts, J. Mol. Catal. A Chem. 167 (2001) 91–99, https://doi.org/10.1016/S1381-1169(00)00495-7.

[32] B. Ravel, M. Newville, ATHENA, ARTEMIS, HEPHAESTUS: data analysis for X-ray absorption spectroscopy using IFEFFIT, J. Synchrotron Radiat. 12 (4) (2005) 537–541, https://doi.org/10.1107/S0909049505012719.

[33] P. Bazin, O. Saur, J.C. Lavalley, M. Daturi, G. Blanchard, FT-IR study of CO adsorption on Pt/CeO 2: characterisation and structural rearrangement of small Pt particles, Phys. Chem. Chem. Phys. 7 (2005) 187–194, https://doi.org/10.1039/b414159h.

[34] A. Beck, P. Rzepka, K.P. Marshall, D. Stoian, M.G. Willinger, J.A. Van Bokhoven, Hydrogen interaction with oxide supports in the presence and absence of platinum, J. Phys. Chem. C 126 (41) (2022) 17589–17597, https://doi.org/10.1021/acs.jpcc.2c05478.

[35] J.L. Carter, P.J. Lucchesi, P. Corneil, D.J.C. Yates, J.H. Sinfelt, Exchange of deuterium with the hydroxyl groups of alumina, J. Phys. Chem. 69 (9) (1965) 3070–3074, https://doi.org/10.1021/j100893a042.

[36] G. Jacobs, Water-gas shift: comparative screening of metal promoters for metal/ceria systems and role of the metal, Appl. Catal. A Gen. 258 (2) (2004) 203–214, https://doi.org/10.1016/j.apcata.2003.09.007.

[37] Z. Yang, G. Luo, Z. Lu, T.K. Woo, K. Hermansson, Structural and electronic properties of NM-doped Ceria (NM = Pt, Rh): a first-principles study, J. Phys. Condens. Matter 20 (3) (2008), 035210, https://doi.org/10.1088/0953-8984/20/03/035210.

[38] A. Bruix, A. Migani, G.N. Vayssilov, K.M. Neyman, J. Libuda, F. Illas, Effects of deposited Pt particles on the reducibility of CeO2(111), Phys. Chem. Chem. Phys. 13 (23) (2011) 11384–11392, https://doi.org/10.1039/c1cp20950g.

[39] F. Coloma, A. Sepu, F. Rodrı, Effect of the presence of chlorine in bimetallic PtZn /CeO2 catalysts for the vapor-phase hydrogenation of crotonaldehyde, Appl. Catal. A Gen. 304 (2006) 159–167, https://doi.org/10.1016/j.apcata.2006.02.039.

[40] J.A. Rodriguez, J.C. Hanson, A.I. Frenkel, J.Y. Kim, M. Pérez, Experimental and theoretical studies on the reaction of H2 with NiO: role of O vacancies and mechanism for oxide reduction, J. Am. Chem. Soc. 124 (2) (2002) 346–354, https://doi.org/10.1021/ja0121080.

[41] C.P. Hwang, C.T. Yeh, Platinum-oxide species formed by oxidation of platinum crystallites supported on alumina, J. Mol. Catal. A Chem. 112 (2) (1996) 295–302, https://doi.org/10.1016/1381-1169(96)00127-6.

[42] J.Z. Shyu, K. Otto, Characterization of Pt/Gamma-alumina catalysts containing ceria, J. Catal. 115 (1989) 16–23, https://doi.org/10.1016/0021-9517(89)90003-1.

[43] A.C.S.F. Santos, S. Damyanova, G.N.R. Teixeira, L.V. Mattos, F.B. Noronha, F. B. Passos, J.M.C. Bueno, The effect of ceria content on the performance of Pt/CeO2/Al2O3 catalysts in the partial oxidation of methane, Appl. Catal. A Gen. 290 (2005) 123–132, https://doi.org/10.1016/j.apcata.2005.05.015.

[44] E.O. Jardim, S. Rico-francés, F. Coloma, J.A. Anderson, J. Silvestre-albero, A. Sepúlveda-escribano, Influence of the metal precursor on the Catalytic Behavior of Pt / ceria catalysts in the preferential oxidation of CO in the presence of H 2 (PROX), J. Colloid Interface Sci. 443 (2015) 45–55, https://doi.org/10.1016/j.jcis.2014.12.013.

[45] S. Salasc, V. Perrichon, M. Primet, M. Chevrier, F. Mathis, N. Moral, Â.C.B. Lyon, Magnetic study of the interaction of hydrogen with a Pt/CeO2 ± Al2O 3 catalyst: influence of the presence of chlorine, Catal. Today 50 (1999) 227–235.

[46] S. Damyanova, J.M.C. Bueno, Effect of CeO2 loading on the surface and catalytic behaviors of CeO2 -Al2O3 -Supported Pt catalysts, Appl. Catal. A Gen. 253 (2003) 135–150, https://doi.org/10.1016/S0926-860X(03)00500-3.

[47] A.D. Allian, K. Takanabe, K.L. Fujdala, X.X. Hao, T.J. Truex, J. Cai, C. Buda, M. Neurock, E. Iglesia, Chemisorption of CO and mechanism of CO oxidation on supported platinum nanoclusters, J. Am. Chem. Soc. 133 (2011) 4498–4517, https://doi.org/10.1021/ja110073u.

[48] H.A. Aleksandrov, K.M. Neyman, I. Hadjiivanov, G.N. Vayssilov, Can the state of platinum species be unambiguously determined by the stretching frequency of an adsorbed CO probe molecule? Phys. Chem. Chem. Phys. 18 (2016) 22108–22121, https://doi.org/10.1039/C6CP03988J.

[49] V. Johánek, F. Dvor, O. Stetsovych, Y. Lykhach, V. Matolín, J. Libuda, Adsorption sites, metal-support interactions, and oxygen spillover identified by vibrational spectroscopy of adsorbed CO: a model study on Pt /ceria catalysts, J. Catal. 289 (2012) 118–126, https://doi.org/10.1016/j.jcat.2012.01.022.

[50] K. Herz, E.J. Shinouskis, Transient oxidation and reduction of alumina supported platinum, Appl. Surf. Sci. 19 (1984) 373–397, https://doi.org/10.1016/0378-5963(84)90074-6.

[51] A. Badri, C. Binet, J. Lavalley, Surface-chlorinated ceria and chlorine-containing reduced Pd / CeO 2 catalysts. A FTIR study, J. Phys. Chem. 100 (20) (1996) 8363–8368.

[52] R. Mandapaka, G. Madras, Zinc and platinum Co-doped ceria for WGS and CO Oxidation, Appl. Catal. B Environ. 211 (2017) 137–147.

[53] P.J.S. Prieto, A.P. Ferreira, P.S. Haddad, D. Zanchet, J.M.C. Bueno, Designing Pt nanoparticles supported on CeO 2 – Al 2 O 3: synthesis, characterization and catalytic properties in the steam reforming and partial oxidation of methane, J. Catal. 276 (2010) 351–359, https://doi.org/10.1016/j.jcat.2010.09.025.

[54] J.M.C. Bueno, B.A. Riguetto, S. Damyanova, G. Gouliev, C.M.P. Marques, L. Petrov, Surface behavior of alumina-supported Pt catalysts modified with cerium as revealed by X-Ray diffraction, X-ray photoelectron spectroscopy, and fourier transform infrared spectroscopy of CO adsorption, J. Phys. Chem. B 108 (17) (2004) 5349–5358, https://doi.org/10.1021/jp031167s.

[55] J. Xu, J.T. Yates, Terrace width effect on adsorbate vibrations: a comparison of Pt (335) and Pt (112) for chemisorption of CO, Surf. Sci. 327 (1995) 193–201.

[56] P. Bera, K.R. Priolkar, A. Gayen, P.R. Sarode, M.S. Hegde, S. Emura, R. Kumashiro, V. Jayaram, G.N. Subbanna, Ionic dispersion of Pt over CeO2 by the combustion method: structural investigation by XRD, TEM, XPS, and EXAFS, Chem. Mater. 15 (10) (2003) 2049–2060, https://doi.org/10.1021/cm0204775.

[57] E.M.C. Alayon, J. Singh, M. Nachtegaal, M. Harfouche, J. A. Van Bokhoven, In situ XAS probes partially oxidized platinum generating high activity for CO oxidation,

[58] N. Marinkovic, K. Sasaki, R. Adzic, Nanoparticle size evaluation of catalysts by EXAFS: advantages and limitations, Zast. Mater. 57 (1) (2016) 101–109, https://doi.org/10.5937/ZasMat1601101M.

[59] J.T. Miller, A.J. Kropf, Y. Zha, J.R. Regalbuto, L. Delannoy, C. Louis, E. Bus, J. A. van Bokhoven, The effect of gold particle size on Au{single Bond}Au bond length and reactivity toward oxygen in supported catalysts, J. Catal. 240 (2) (2006) 222–234, https://doi.org/10.1016/j.jcat.2006.04.004.

[60] M. Vaarkamp, J.T. Miller, F.S. Modica, D.C. Koningsberger, On the relation between particle morphology, structure of the metal-support interface, and catalytic properties of Pt/ γ-Al2O3, J. Catal. 163 (2) (1996) 294–305, https://doi.org/10.1006/jcat.1996.0330.

[61] H.H. Liu, Y. Wang, A.P. Jia, S.Y. Wang, M.F. Luo, J.Q. Lu, Oxygen vacancy promoted CO oxidation over Pt/CeO2 catalysts: a reaction at Pt-CeO2 interface, Appl. Surf. Sci. 314 (2014) 725–734, https://doi.org/10.1016/j.apsusc.2014.06.196.

[62] D.W. Daniel, Infrared studies of CO and CO₂ adsorption on Pt/CeO2: the characterization of active sites, J. Phys. Chem. 4487 (1988) 3891–3899, https://doi.org/10.1002/chin.198838025.

[63] F. Stoop, F.J.C.M. Toolenaar, V. Ponec, Geometric and ligand effects in the infrared spectra of adsorbed carbon monoxide, J. Catal. 73 (1982) 50–56, https://doi.org/10.1016/0021-9517(82)90079-3.

[64] E. Bus, J.T. Miller, a J. Kropf, R. Prins, J. a van Bokhoven, Analysis of in situ EXAFS data of supported metal catalysts using the third and fourth cumulant, Phys. Chem. Chem. Phys. 8 (27) (2006) 3248–3258, https://doi.org/10.1039/b605248g.

[65] K. Heinemann, H. P, In situ TEm evidence of lattice expansion of very small supported palladium particles, Surf. Sci. 156 (1985) 265–274, https://doi.org/10.1016/0039-6028(85)90583-7.

[66] A. Migani, G.N. Vayssilov, S.T. Bromley, K.M. Neyman, Dramatic reduction of the oxygen vacancy formation energy in ceria particles: a possible key to their remarkable reactivity at the nanoscale, J. Mater. Chem. 20 (2010) 10535–10546, https://doi.org/10.1039/c0jm01908a.

[67] F. Coloma, A. Sepu, F. Rodrı, Effect of the presence of chlorine in bimetallic PtZn /CeO 2 catalysts for the vapor-phase hydrogenation of crotonaldehyde, Appl. Catal. A Gen. 304 (2006) 159–167, https://doi.org/10.1016/j.apcata.2006.02.039.

[68] R.A. Daley, S.Y. Christou, A.M. Efstathiou, J.A. Anderson, Influence of oxychlorination treatments on the redox and oxygen storage and release properties of thermally Aged Pd-Rh/CexZr1-XO 2/Al2O3 model three-way catalysts, Appl. Catal. B Environ. 60 (1–2) (2005) 117–127, https://doi.org/10.1016/j.apcatb.2005.03.002.

[69] J.A. Anderson, R.A. Daley, S.Y. Christou, A.M. Efstathiou, Regeneration of thermally aged Pt-Rh/CexZr1-XO2-Al2O3 model three-way catalysts by oxychlorination treatments, Appl. Catal. B Environ. 64 (3–4) (2006) 189–200, https://doi.org/10.1016/j.apcatb.2005.12.007.

[70] F.J. Gracia, J.T. Miller, A.J. Kropf, E.E. Wolf, Kinetics, FTIR, and controlled atmosphere EXAFS study of the effect of chlorine on Pt-supported catalysts during oxidation reactions, J. Catal. 209 (2002) 341–354, https://doi.org/10.1006/jcat.2002.3601.

[71] F. Normand, Le, L. Hilaire, K. Kili, G. Krill, G. Mairet, Oxidation state of cerium in cerium-based catalysts investigated by spectroscopic probes, J. Phys. Chem. 92 (9) (1988) 2561–2568.

[72] R.J. Gorte, S. Zhao, Studies of the water-gas-shift reaction with ceria-supported precious metals, Catal. Today 104 (1) (2005) 18–24, https://doi.org/10.1016/j.cattod.2005.03.034.

[73] C. Vignatti, M.S. Avila, C.R. Apesteguía, T.F. Garetto, Catalytic and DRIFTS study of the WGS reaction on Pt-based catalysts, Int. J. Hydrogen Energy 35 (14) (2010) 7302–7312, https://doi.org/10.1016/j.ijhydene.2010.04.180.

[74] J. Vecchietti, A. Bonivardi, W. Xu, D.J. Stacchiola, J.J. Delgado, M. Calatayud, S. E. Collins, Understanding the role of oxygen vacancies in the water gas shift reaction on ceria-supported platinum catalysts, ACS Catal. 4 (2014) 2088–2096, https://doi.org/10.1021/cs500323u.

[75] C.M. Kalamaras, S. Americanou, A.M. Efstathiou, "Redox" vs "associative formate with -OH group regeneration" WGS reaction mechanism on Pt/CeO2: effect of platinum particle size, J. Catal. 279 (2011) 287–300, https://doi.org/10.1016/j.jcat.2011.01.024.

[76] Y. Li, M. Kottwitz, J.L. Vincent, M.J. Enright, Z. Liu, L. Zhang, J. Huang, S. D. Senanayake, W.C.D. Yang, P.A. Crozier, R.G. Nuzzo, A.I. Frenkel, Dynamic structure of active sites in ceria-supported Pt catalysts for the water gas shift reaction, Nat. Commun. 12 (1) (2021) 1–9, https://doi.org/10.1038/s41467-021-21132-4.

[77] A. Bruix, J. a Rodriguez, P.J. Ramírez, S.D. Senanayake, J. Evans, J.B. Park, D. Stacchiola, P. Liu, J. Hrbek, F. Illas, A new type of strong metal-support interaction and the production of H2 through the transformation of water on Pt/CeO2(111) and Pt/CeO(x)/TiO2(110) catalysts, J. Am. Chem. Soc. 134 (21) (2012) 8968–8974, https://doi.org/10.1021/ja302070k.

[78] Y. Suchorski, R. Wrobel, S. Becker, H. Weiss, CO oxidation on a CeO / Pt (111) inverse model catalyst surface: catalytic promotion and tuning of kinetic phase diagrams, J. Phys. Chem. C 112 (111) (2008) 20012–20017.

[79] A. Jentys, Estimation of mean size and shape of small metal particles by EXAFS, Phys. Chem. Chem. Phys. 1 (17) (1999) 4059–4063, https://doi.org/10.1039/A904654B.

[80] S. Aranifard, S.C. Ammal, A. Heyden, On the importance of the associative carboxyl mechanism for the water-gas shift reaction at Pt / CeO 2 interface sites, J. Phys. Chem. 118 (2014) 634–6323.

[81] G. Pirug, H.P. Bonzel, G. Brodén, The adsorption of posatssiul on Pt(111) and its effect on oxygen adsorption, Surf. Sci. 122 (1982) 1–20.

[82] M. González-Castaño, S. Ivanova, T. Ioannides, M.A. Centenoa, A.O. J, Deep insight into Zr/Fe combination for successful Pt/CeO2/Al2O3 WGS catalyst doping, Catal. Sci. Technol. 7 (2017) 1556–1564, https://doi.org/10.1039/C6CY02551J.